The exact Laplacian spectrum for the Dyson hierarchical network

Elena Agliari[1] and Flavia Tavani[2]

[1]*Dipartimento di Matematica, Sapienza Università di Roma, P.le A. Moro 2, 00185, Roma, Italy.*
[2]*Dipartimento SBAI (Ingegneria), Sapienza Università di Roma, via A. Scarpa 16, 00161, Roma, Italy.*

(Dated: April 21, 2016)

We consider the Dyson hierarchical graph $\mathcal{G}$, that is a weighted fully-connected graph, where the pattern of weights is ruled by the parameter $\sigma \in (1/2, 1]$. Exploiting the deterministic recursivity through which $\mathcal{G}$ is built, we are able to derive explicitly the whole set of the eigenvalues and the eigenvectors for its Laplacian matrix. Given that the Laplacian operator is intrinsically implied in the analysis of dynamic processes (e.g., random walks) occurring on the graph, as well as in the investigation of the dynamical properties of connected structures themselves (e.g., vibrational structures and the relaxation modes), this result allows addressing analytically a large class of problems. In particular, as examples of applications, we study the random walk and the continuous-time quantum walk embedded in $\mathcal{G}$, and the relaxation times of a polymer whose structure is described by $\mathcal{G}$.

PACS numbers:

arXiv:1604.05864v1 [physics.data-an] 20 Apr 2016

I. INTRODUCTION

Most real-life networks display non-trivial features concerning their topological structure as well as the pattern of weights associated to their links. In fact, the arrangement of the connections between their constituent elements is typically neither purely regular nor purely random and, also, such connections are associated to weights accounting for wiring costs which typically depends on the distance (e.g., a physical distance, a social distance) between elements to be linked [1, 2, 3, 4, 5, 6].

As well known, the topology and the distribution of weights have strong influence on the dynamical properties of the structure and on the dynamical properties of processes embedded in the structure itself. This is the case, for instance, for the dynamics of polymer networks (e.g., their response to external forces [7]), for diffusion and transport processes (e.g., epidemics in social networks [8], chemical-kinetics [9], quantum search algorithms [10]), for statistical mechanics models (e.g., ferromagnetic systems [11, 12], glasses [13] and neural networks [14]).

Now, the topology and the pattern of weights of a given structure can be mathematically captured in terms of the Laplacian matrix, and most dynamical properties can be fully described through the Laplacian eigenvectors and eigenvalues (see e.g., the review [15, 16, 17, 18, 19, 20]). Also, recent developments have shown how to approach analytically the solution of spin systems via methods based on the extension of the replica method where both the degrees (via hard constraints) and the matrix spectrum (via a soft constraint) are prescribed [21].

Beyond the above mentioned physically-driven applications, the study of the graph spectrum realizes increasingly rich connections with many other areas of mathematics; a particularly important development is the interaction between spectral graph theory and differential geometry (see e.g., [19, 22]). As a result, during the past few decades, the study of Laplacian eigenvalues has attracted an upsurge of interest. Among the (deterministic) structures for which the full knowledge of the spectrum has been achieved we can mention several examples of fractals [23, 24], of small-world networks [25], and of scale-free graphs [26], just to cite a few. However, in general, deriving the exact Laplacian spectrum for an arbitrary system is a challenging task and the use of deterministic structures is of much help to this aim.

Here we focus on a particular example of weighted graph and we derive analytically its Laplacian spectrum. More precisely, the graph considered is a weighted, fully-connected network, originally introduced by Dyson [27] to mimic a one-dimensional structure with long-range interactions. In fact, the weight J_{ij} associated to the link connecting node i and node j scales as $J_{ij} \sim 4^{-d_{ij}\sigma}$, where d_{ij} is the distance between the nodes considered and σ is a positive tunable parameter that rules the decay of the interaction between nodes as their distance varies. This network is built deterministically and recursively, and we show that, given its building procedure, the coupling matrix $\mathbf{J}$ exhibits a block form which allows the analytical investigation of its spectrum. In fact, we are able to derive the full, exact Laplacian spectrum as well as its eigenvectors.

These findings can be exploited in a wide range of problems, from structural problems, such as the determination of the spanning trees, of the resistance distance and of the community structures, to dynamical problems as those mentioned above. In particular, here, we address a few applications concerning several different fields to show the effectiveness of the Laplacian spectrum.

First, we calculate the mean first passage time for a random walker embedded in $\mathcal{G}$, finding that the average mean

time to first reach a given node depends functionally on σ and it grows as the inhomogeneity of the pattern of weights is enhanced.
Also, we consider a quantum particle moving in a potential described by $\mathcal{G}$ (namely the Hamiltonian which determines the time evolution is identified by the Laplacian of $\mathcal{G}$) and we calculate the long-time average, finding that, in the limit of large size, it converges to $1/3$, much above the equipartition limit $1/N$ expected for classical propagation, hence suggesting that $\mathcal{G}$ is not well performing as far as coherent propagation is concerned.
Finally, we consider $\mathcal{G}$ in the framework of generalized Gaussian structures and, based on the spectra, we calculate the structural average of the mean monomer displacement under applied constant force and the mechanical relaxation moduli, again highlighting the role of inhomogeneity in the coupling pattern.

The paper is organized as follows. In Sec. II we review the basic definitions concerning the Laplacian matrix and in Sec. III we review the hierarchical structure considered, discussing its building procedure and the block structure of its coupling matrix. Then, in Secs. IV and V we derive analytically the eigenvalues and the eigenvectors, respectively, of the Laplacian matrix for the hierarchical graph considered, while in Sec. VI we exploit these findings to derive some results concerning applications in several field. Finally, Sec. VII is left for conclusions, remarks and outlooks.

II. THE LAPLACIAN SPECTRUM AND ITS APPLICATIONS

The Laplacian matrix has a long history in science and there are several books and survey papers dealing with its mathematical properties and applications, see e.g., [15, 16, 17, 18, 19, 20]. Here we just review some basic definitions in order to provide a background for the following analysis.

Let $\mathbf{J}$ be the generalized adjacency matrix (weight matrix) of a graph $\mathcal{G}$ of size N, in such a way that the entry J_{ij} of $\mathbf{J}$ is non null if i and j are adjacent in $\mathcal{G}$, otherwise J_{ij} is zero. We call w_i the weighted degree of node i which is defined as $w_i \equiv \sum_{j=1}^{N} J_{ij}$. Further, let $\mathbf{W}$ be the diagonal matrix, whose entries are given by $W_{ij} = w_i \delta_{ij}$. The Laplacian matrix of $\mathcal{G}$ is then defined as

$$\mathbf{L} = \mathbf{W} - \mathbf{J}. \tag{1}$$

Given that $\mathbf{L}$ is semi-definite positive, the Laplacian eigenvalues are all real and non-negative. Also, they are contained in the interval $[0, \min\{N, 2w_{\max}\}]$, where $w_{\max}$ is the maximum weighted degree of $\mathcal{G}$. The set of all N Laplacian eigenvalues $\lambda_1 \leq \lambda_2 \leq ... \leq \lambda_N$ is called the Laplacian spectrum. Following the definition (1), the smallest eigenvalue λ_1 is always null and corresponds to the eigenvector $\mu_1 = \mathbf{e}_N$, according to the Frobenous-Perron theorem. The second smallest eigenvalue is $\lambda_2 \geq 0$, and it equals zero only if the graph is disconnected. Thus, the multiplicity of 0 as an eigenvalue of $\mathbf{L}$ corresponds to the number of components of $\mathcal{G}$.

The smallest non-zero Laplace eigenvalue is often referred to as "spectral gap" (or also "algebraic connectivity") and it provides information on the effective bipartitioning of a graph. Basically, a graph with a "small" first non-trivial Laplacian eigenvalue has a relatively clean bisection (i.e., the smaller the spectral gap and the smaller the relative number of edges required to be cut away to generate a bipartition), conversely, a large spectral gap characterizes non-structured networks, with poor modular structure (see e.g., [28, 29]).

The spectral gap has also remarkable effects on dynamical processes. For instance, let us consider a system of N oscillators represented by the nodes of $\mathcal{G}$, which are interconnected pairwise by means of active links; the time evolution of the i-th oscillator is given by $\dot{x}_i = F(x_i) - \beta \sum_{j=1}^{N} L_{ij} H(x_j)$, where F and H are the evolution and the output functions, respectively, and β is a coupling constant. In this case it has been shown that a network exhibits good synchronizability if the eigenratio λ_N/λ_2 is as small as possible [30]. A small spectral gap is therefore likely to imply a poor synchronizability.

However, probably the easiest dynamical process affected by the underlying topology is the random walk. In this context, the spectral gap is associated with spreading efficiency: random walks move around quickly and disseminate fluently on graphs with large spectral gap in the sense that they are very unlikely to stay long within a given subset of vertices unless its complementary subgraph is very small [31].

Finally, we just mention at the relation between the number of spanning trees in a graph $\mathcal{G}$ and its Laplacian spectrum. Let us denote with $\Omega(\mathcal{G})$ the number of spanning trees in $\mathcal{G}$: the Kirchhoff matrix-tree theorem states that (see e.g., [32, 33]) $\Omega(\mathcal{G}) = N^{-1} \prod_{k=2}^{N} \lambda_k$. This formula turns out to be extremely useful in order to get bounds for $\Omega(\mathcal{G})$ even without having the exact spectrum of the related graph, or in order to estimate the number of spanning trees of complex graphs which can be defined as combinations of simpler graphs for which the exact spectrum is known (see e.g., [34]). Beyond the purely mathematical point of view, deriving $\Omega(\mathcal{G})$ is a key problem in many areas of experimental design for the synthesis of reliable communication networks where the links of the network are subject to failure [35].

Further applications will be reviewed and deepened in Sec. VI for the particular graph considered here.

III. DESCRIPTION OF THE HIERARCHICAL NETWORK

In this work we focus on a deterministic, weighted, recursively grown graph, referred to as $\mathcal{G}$, originally introduced by Dyson to study the statistical-mechanics of spin systems beyond the mean-field scenario [27]. The topological properties of this graph have been discussed in [14, 36, 37], and here we briefly review them. The construction begins with 2 nodes, connected with a link carrying a weight $J(1,1,\sigma) = 4^{-\sigma}$. We refer to this graph as $\mathcal{G}_1$, and in the notation $J(d,k,\sigma)$ we highlight the dependence on the graph iteration k and on the system parameter σ, also, d represents the iteration when the nodes considered first turn out to be connected. At the next step, one takes two replicas of $\mathcal{G}_1$ and connects the nodes pertaining to different replicas with links displaying a weight $J(2,2,\sigma) = 4^{-2sigma}$; moreover, the weight on the existing links is updated as $J(1,1,\sigma) \to J(1,2,\sigma) = J(1,1,\sigma) + J(2,2,\sigma)$. This realizes the graph $\mathcal{G}_2$, which counts overall 4 nodes. At the generic k-th iteration, one takes two replicas of $\mathcal{G}_{k-1}$, insert 2^{2k-1} new links, each carrying a weight $J(k,k,\sigma) = 4^{-k\sigma}$, among nodes pertaining to different replicas, and the weights on existing links are updated as $J(d,k-1,\sigma) \to J(d,k,\sigma) = J(d,k-1,\sigma) + J(k,k,\sigma)$, for any $d < k$. If we stop the iterative procedure at the K-th iteration, the final graph $\mathcal{G}_K$ counts $N = 2^K$ nodes and the coupling between any pair of nodescan be expressed as

$$J(d,K,\sigma) = \sum_{l=d}^{K} J(l,K,\sigma) = \sum_{l=d}^{K} 4^{-l\sigma} = \frac{4^{\sigma(1-d)} - 4^{-K\sigma}}{4^{\sigma} - 1}, \tag{2}$$

with $d \in \{1,...,K\}$. Remarkably, this iterative procedure allows for a definition of metric[1]: two nodes are said to be at distance d if they occur to be first connected at the d-th iteration. As a result, we can define a coupling matrix $\mathbf{J}$ associated to the network $\mathcal{G}_K$ such that the entry J_{ij} depends on the nodes (i,j) considered only through their distance d_{ij}, namely

$$J_{ij} = \frac{4^{\sigma(1-d_{ij})} - 4^{-K\sigma}}{4^{\sigma} - 1}. \tag{3}$$

Given the building procedure of $\mathcal{G}_K$, a generic node i has 2^{d-1} nodes at distance $d \in \{1,...,K\}$. Moreover, the total weight of the links stemming from a single node i can be written as

$$\begin{aligned} w_i &= \sum_{i \neq j} J_{ij} = \sum_{l=1}^{K} 2^{d-1} J(d,K,\sigma) = \\ &= \frac{2N^{1-2\sigma}(1-2^{2\sigma}) + N^{-2\sigma}(2^{2\sigma}-2) + 2^{2\sigma}}{(2^{2\sigma}-1)(2^{2\sigma}-2)}. \end{aligned} \tag{4}$$

Due to the homogeneity of the network, w_i does not depend on the site i, so one can simply write $w_i = w$.

Beyond the coupling matrix $\mathbf{J}$, one can introduce the Laplacian matrix $\mathbf{L}$, which, as anticipated, is defined as

$$\mathbf{L} = \mathbf{W} - \mathbf{J}, \tag{5}$$

where $\mathbf{W}$ is a diagonal matrix with elements $W_{ij} = w\delta_{ij}$.

---

[1] One can check that this metric is intrinsically ultrametric since, beyond the standard conditions for a well defined metric ($d_{ij} \geq 0$; $d_{ij} = 0 \Leftrightarrow i = j$; $d_{ij} = d_{ji}$), the so-called ultrametric inequality ($d_{ij} \leq \max(d_{iz}, d_{zj})$) also holds.

IV. EIGENVALUES OF THE DYSON HIERARCHICAL GRAPH

In order to get familiar with the structure of the matrix $\mathbf{J}$, it is convenient to write it down explicitly for a small value of K. In particular, for $K = 3$ it reads as

$$\mathbf{J}^{(N)} = \left(\begin{array}{cccc|cccc} 0 & \sum_{i=1}^{3} t^i & \sum_{i=2}^{3} t^i & \sum_{i=2}^{3} t^i & t^3 & t^3 & t^3 & t^3 \\ \sum_{i=1}^{3} t^i & 0 & \sum_{i=2}^{3} t^i & \sum_{i=2}^{3} t^i & t^3 & t^3 & t^3 & t^3 \\ \sum_{i=2}^{3} t^i & \sum_{i=2}^{3} t^i & 0 & \sum_{i=1}^{3} t^i & t^3 & t^3 & t^3 & t^3 \\ \sum_{i=2}^{3} t^i & \sum_{i=2}^{3} t^i & \sum_{i=1}^{3} t^i & 0 & t^3 & t^3 & t^3 & t^3 \\ \hline t^3 & t^3 & t^3 & t^3 & 0 & \sum_{i=1}^{3} t^i & \sum_{i=2}^{3} t^i & \sum_{i=2}^{3} t^i \\ t^3 & t^3 & t^3 & t^3 & \sum_{i=1}^{3} t^i & 0 & \sum_{i=2}^{3} t^i & \sum_{i=2}^{3} t^i \\ t^3 & t^3 & t^3 & t^3 & \sum_{i=2}^{3} t^i & \sum_{i=2}^{3} t^i & 0 & \sum_{i=1}^{3} t^i \\ t^3 & t^3 & t^3 & t^3 & \sum_{i=2}^{3} t^i & \sum_{i=2}^{3} t^i & \sum_{i=1}^{3} t^i & 0 \end{array}\right), \tag{6}$$

where we posed $t = 4^{-\sigma}$ and we highlighted with the super-index N the size of the matrix; in general, $N = 2^K$ and here $N = 8$. The block structure is evident and can be schematised as

$$\mathbf{J}^{(N)} = \left(\begin{array}{c|c} \mathbf{L}^{(N/2)} & \mathbf{R}^{(N/2)} \\ \hline \mathbf{R}^{(N/2)} & \mathbf{L}^{(N/2)} \end{array}\right), \tag{7}$$

where $\mathbf{L}$ and $\mathbf{R}$ are square matrices of size $\frac{N}{2} \times \frac{N}{2}$. For such matrices, the determinant can be computed as

$$\det(\mathbf{J}^{(N)}) = \det(\mathbf{L}^{(N/2)} - \mathbf{R}^{(N/2)}) \det(\mathbf{L}^{(N/2)} + \mathbf{R}^{(N/2)}). \tag{8}$$

Using the ultrametric structure of $\mathbf{J^{(N)}}$, we can iterate this block decomposition. In fact, for example, after the first decomposition we obtain two matrices $\mathbf{J}_1^{N/2}$ and $\mathbf{J}_2^{N/2}$ such that

$$\mathbf{J_1}^{(N/2)} \equiv \mathbf{L}^{(N/2)} - \mathbf{R}^{(N/2)} = \left(\begin{array}{c|c} \mathbf{L_1}^{(N/4)} & \mathbf{R_1}^{(N/4)} \\ \hline \mathbf{R_1}^{(N/4)} & \mathbf{L_1}^{(N/4)} \end{array}\right), \qquad \mathbf{J_2}^{(N/2)} \equiv \mathbf{L}^{(N/2)} + \mathbf{R}^{(N/2)} = \left(\begin{array}{c|c} \mathbf{L_2}^{(N/4)} & \mathbf{R_2}^{(N/4)} \\ \hline \mathbf{R_2}^{(N/4)} & \mathbf{L_2}^{(N/4)} \end{array}\right). \tag{9}$$

Now, both $\mathbf{J_1}^{(N/2)}$ and $\mathbf{J_2}^{(N/2)}$ display the same block structure and for each an expression analogous to (8) holds in such a way that

$$\det(\mathbf{J}^{(N)}) = \det(\mathbf{L_1}^{(N/4)} - \mathbf{R_1}^{(N/4)}) \det(\mathbf{L_1}^{(N/4)} + \mathbf{R_1}^{(N/4)}) \det(\mathbf{L_2}^{(N/4)} - \mathbf{R_2}^{(N/4)}) \det(\mathbf{L_2}^{(N/4)} + \mathbf{R_2}^{(N/4)}). \tag{10}$$

At this point, we pose

$$\begin{aligned} \mathbf{J_1}^{(N/4)} &\equiv \mathbf{L_1}^{(N/4)} - \mathbf{R_1}^{(N/4)} \\ \mathbf{J_2}^{(N/4)} &\equiv \mathbf{L_1}^{(N/4)} + \mathbf{R_1}^{(N/4)} \\ \mathbf{J_3}^{(N/4)} &\equiv \mathbf{L_2}^{(N/4)} - \mathbf{R_2}^{(N/4)} \\ \mathbf{J_4}^{(N/4)} &\equiv \mathbf{L_2}^{(N/4)} + \mathbf{R_2}^{(N/4)} \end{aligned}$$

where, as stated previously, the super-index indicates the size of the matrices and, proceeding iteratively, we get a set of $N/2$ matrices of size 2×2 and referred to as $\{\mathbf{J}_l^{(2)}\}$ with $l = 1, ..., N/2$.
More precisely, at every n-th iteration, we can write 2^n block matrices $\{\mathbf{J}_l^{(N/2^n)}\}_{l=1}^{2^n}$ of size $N/2^n$, $n = 1, ...K-1$, obtained as the sum or the difference of the 2^{n-1} matrices of the previous iteration. With this argument, we can state that our determinant is a product of $N/2$ determinants of matrices 2×2 as

$$\det(\mathbf{J}^{(N)}) = \prod_{n=1}^{N/2} \det \mathbf{J}_n{}^{(2)}. \tag{11}$$

Clearly, in order to compute the eigenvalues of $\mathbf{J}$, we can again use this scheme, but taking as initial matrix $\mathbf{J} - \lambda\mathbf{I}$. In this case, with some algebra, we obtain the following

$$\det(\mathbf{J} - \lambda\mathbf{I}) = \prod_{n=1}^{K} p_n, \tag{12}$$

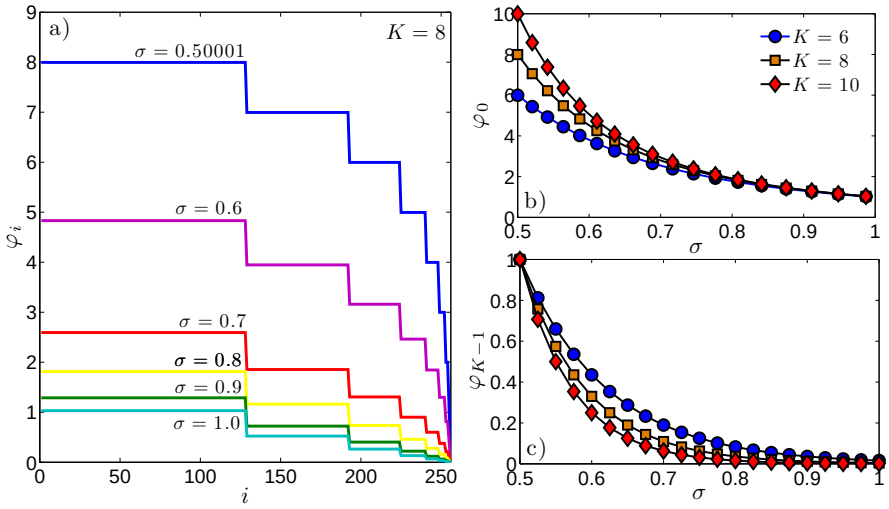

FIG. 1: Panel *a*: Eigenvalue spectrum of $\mathbf{L}$ for $K = 8$ and for different values of σ. The multiplicity of an eigenvalue corresponds to a plateau and it grows with the magnitude of the eigenvalue. Moreover, the spectrum is broadened over a range which grows with σ. Panel *b*: trend of the eigenvalue φ_0 when σ varies in the interval $(1/2, 1]$ for different values of K as shown in the legend. Since φ_0 corresponds to the largest eigenvalue this also provides the span of the spectrum itself. Panel *c*: trend of the eigenvalue φ_{K-1} when σ varies in the interval $(1/2, 1]$ for different values of K (the legend is the same as panel *b*). Since φ_{K-1} corresponds to the smallest non-null eigenvalue this also provides the spectral gap for $\mathcal{G}_K$.

where p_n is the determinant of a proper matrix of size $N/2^n \times N/2^n$ and it reads as

$$p_n = \left\{ \left[-\lambda + \sum_{l=2}^{n} (2^{l-1} - 1) t^l - \sum_{l=n+1}^{K} t^l \right]^2 - \left(\sum_{l=1}^{n} 2^{l-1} t^l \right)^2 \right\}^{\frac{N}{2^{n+1}}}, \qquad n = 1, \cdots, K. \tag{13}$$

By plugging the previous expression for p_n into Eq. 12 and solving for the roots of $\det(\mathbf{J} - \lambda \mathbf{I}) = 0$, we get $K + 1$ distinct eigenvalues that can be written as

$$\lambda_n = \frac{N^{-2\sigma}(2^{2\sigma} - 2) - 2 \times 2^{n(1-2\sigma)}(2^{2\sigma} - 1) + 2^{2\sigma}}{(2^{2\sigma} - 1)(2^{2\sigma} - 2)}, \quad n = 0, \cdots, K-1, \text{ with algebraic multiplicity } \frac{N}{2^{n+1}}, \tag{14}$$

$$\lambda_K = w, \text{ with algebraic multiplicity } 1, \tag{15}$$

One can see that, as n increases, both λ_n and its multiplicity decrease.

Actually, we are mainly interested in the spectrum of the Laplacian matrix $\mathbf{L} = \mathbf{W} - \mathbf{J}$, with $\mathbf{W} = w\delta_{ij}$, where we recall that w is the weighted degree defined in Eq. 4. Now, denoting with φ_n the n-th eigenvalue of $\mathbf{L}$, and exploiting the fact that $\mathbf{W}$ is proportional to the identity matrix, one can write

$$\varphi_n = w - \lambda_n, \qquad n = 0, ..., K. \tag{16}$$

More precisely we have

$$\varphi_n = \frac{2^{n(1-2\sigma)} - N^{1-2\sigma}}{2^{2\sigma-1} - 1} \qquad n = 0, ..., K-1 \text{ with algebraic multiplicity } \frac{N}{2^{n+1}}, \tag{17}$$

$$\varphi_K = 0, \text{ with algebraic multiplicity } 1. \tag{18}$$

Of course, since $\mathbf{L}$ is semidefinite positive, $\varphi_n \geq 0 \ \forall n \geq 0$, and, in particular, omitting the trivial eigenvalue $\varphi_K = 0$, we have

$$\max_{n=0,...,K-1} \varphi_n = \varphi_0 = (1 - N^{1-2\sigma})/(2^{2\sigma-1} - 1) \tag{19}$$

$$\min_{n=0,...,K-1} \varphi_n = \varphi_{K-1} = N^{1-2\sigma}. \tag{20}$$

From Eq. 17 we notice that the higher the value of φ_n, and the higher its algebraic multiplicity (see also Fig. 1, panel *a*). Moreover, from Eq. 19 we see that φ_0 decreases with σ (see Fig. 1, panel *b*) and, as a consequence, the

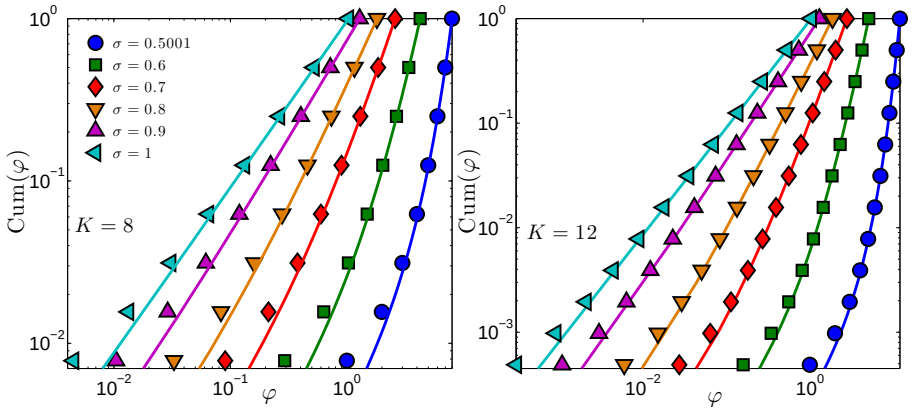

FIG. 2: The cumulative function Cum(φ) defined in Eq. 21 is shown for $K = 8$ (left panel) and $K = 12$ (right panel) and for several choices of σ. Symbols correspond to the numerical estimate of Eq. 21, while solid lines correspond to the theoretical expression in Eq. 23. Notice that, as underlined in the main text, the spectrum spans over a range which shrinks with σ.

spectrum covers a narrower interval as the pattern of couplings gets more homogeneous. Similarly, the spectral gap, corresponding to φ_n, decreases fast with σ (see Fig. 1, panel *c*) and, as a consequence, the spreading efficiency on $\mathcal{G}_K$ is enhanced as the patter of couplings gets more homogeneous.

Equations 17 and 18 provide an explicit expression for the spectrum of the Laplacian matrix associated to the hierarchical graph under study. The distribution $P(\varphi)$ of the Laplacian eigenvalues, returning the fraction of eigenvalues laying in the interval $(\varphi, \varphi + d\varphi)$, can be analytically recovered as follows. First, we determine the cumulative distribution Cum(φ): fixing an arbitrary value $\bar{\varphi} \in [\varphi_K, \varphi_0]$, the overall number of eigenvalues smaller than or equal to $\bar{\varphi}$ is given by

$$\mathrm{Cum}(\bar{\varphi}) = \frac{1}{N} \sum_{n=\lfloor n(\bar{\varphi}) \rfloor}^{K-1} \frac{N}{2^{n+1}}, \tag{21}$$

where $n(\bar{\varphi})$ is obtained by inverting Eq. 17, that is,

$$n(\bar{\varphi}) = \frac{1}{1-2\sigma} \log_2 \left[N^{1-2\sigma} + \bar{\varphi}(2^{2\sigma-1} - 1) \right], \tag{22}$$

and with $\lfloor x \rfloor$ we take the largest integer not greater than x. We stress that $\lfloor n(\bar{\varphi}) \rfloor$ provides the index n such that φ_n is the eigenvalue closest to $\bar{\varphi}$, with $\varphi \leq \bar{\varphi}$. Moreover, we observe that in Eq. 21, the index of the sum varies between $\lfloor n(\bar{\varphi}) \rfloor$ and $K - 1$: this is because, according to the notation introduced in Eq. 17, the eigenvalues decrease as n increases, so to find all the eigenvalues smaller than or equal to a fixed $\bar{\varphi}$, it is necessary to consider the larger indices.

The cumulative distribution Cum(φ) can be calculated merging the results (21) and (22), obtaining

$$\mathrm{Cum}(\varphi) = \left[N^{1-2\sigma} + \varphi(2^{2\sigma-1} - 1) \right]^{\frac{1}{2\sigma-1}} - \frac{1}{N}, \qquad \text{with } \varphi_{\mathrm{lb}} \leq \varphi \leq \varphi_{\mathrm{ub}}, \tag{23}$$

where we called $\varphi_{\mathrm{lb}} = N^{1-2\sigma}$ and $\varphi_{\mathrm{ub}} = (1 - N^{1-2\sigma})/(2^{2\sigma-1} - 1)$ the lower-bound and the upper-bound of φ, respectively. Of course, in the limit $N \to \infty$, Cum(φ_{ub}) and Cum(φ_{lb}) converge to the expected values, being $\mathrm{Cum}(\varphi_{\mathrm{ub}}) = 1 - 1/N \to 1$, and $\mathrm{Cum}(\varphi_{\mathrm{lb}}) = 1/N \to 0$. The expression (23) is numerically checked in Fig. 2.

Finally, taking the derivative of Cum(φ), we get an estimate for $P(\varphi)$:

$$P(\varphi_n) \approx \mathrm{Cum}(\varphi_{n-1}) - \mathrm{Cum}(\varphi_n) \approx -\frac{\partial \mathrm{Cum}(\varphi)}{\partial n} \sim [N^{1-2\sigma} + \varphi(2^{2\sigma-1} - 1)]^{1/(2\sigma-1)}, \tag{24}$$

where in the last passage we used (21). Thus, for large sizes and in the upper part of the spectrum range, where $\varphi \gg N^{1-2\sigma}$, the distribution scales as $P(\varphi) \sim \varphi^{1/(2\sigma-1)}$. This result is checked numerically in Fig. 3.

V. EIGENVECTORS

Having computed the spectrum of $\mathbf{L}$, we can now proceed with the calculation of its eigenvectors. As shown in the previous section, we have $K + 1$ distinct eigenvalues, each with its own algebraic multiplicity. We are looking for a

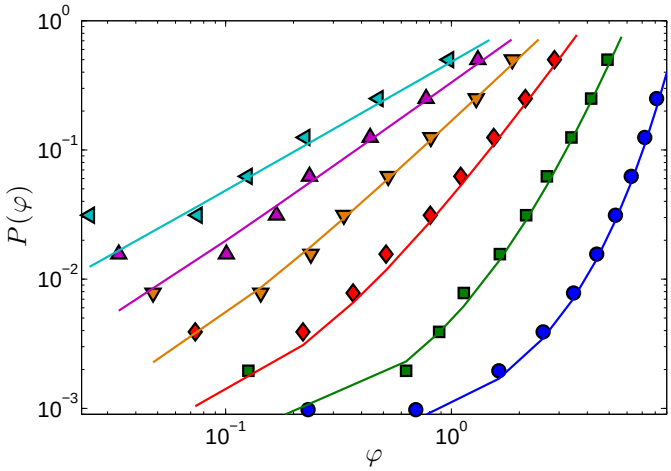

FIG. 3: The eigenvalue distribution $P(\varphi)$ for a system of size $N = 2^K$ with $K = 10$ is shown versus φ and for several choices of σ (the legend is the same as in Fig. 2). We first derived an histogram (symbols) from the exact spectrum and then compare with the theoretical estimate (solid line) given by Eq. 23. The comparison is successful especially for large values of φ.

system of linear independent vectors $\{\mu_i\}_{i=1}^N$, where μ_i is a $N \times 1$ vector such that

$$\mathbf{L}\mu_n = \varphi_n \mu_n \qquad n = 1, .., N, \tag{25}$$

with $\mu_i \mu_j = \delta_{ij}$ and $\| \mu_i \| = 1$, $\forall i = 1, ..., N$.

Again, we can exploit the block structure of $\mathbf{L}$ to find these eigenvectors. In fact, if $K = 3$, and calling again $t = 4^{-\sigma}$, $\mathbf{L}$ has the form

$$\mathbf{L} = \begin{pmatrix} w & -\sum_{i=1}^3 t^i & -\sum_{i=2}^3 t^i & -\sum_{i=2}^3 t^i & -t^3 & -t^3 & -t^3 & -t^3 \\ -\sum_{i=1}^3 t^i & w & -\sum_{i=2}^3 t^i & -\sum_{i=2}^3 t^i & -t^3 & -t^3 & -t^3 & -t^3 \\ -\sum_{i=2}^3 t^i & -\sum_{i=2}^3 t^i & w & -\sum_{i=1}^3 t^i & -t^3 & -t^3 & -t^3 & -t^3 \\ -\sum_{i=2}^3 t^i & -\sum_{i=2}^3 t^i & -\sum_{i=1}^3 t^i & w & -t^3 & -t^3 & -t^3 & -t^3 \\ -t^3 & -t^3 & -t^3 & -t^3 & w & -\sum_{i=1}^3 t^i & -\sum_{i=2}^3 t^i & -\sum_{i=2}^3 t^i \\ -t^3 & -t^3 & -t^3 & -t^3 & -\sum_{i=1}^3 t^i & w & -\sum_{i=2}^3 t^i & -\sum_{i=2}^3 t^i \\ -t^3 & -t^3 & -t^3 & -t^3 & -\sum_{i=2}^3 t^i & -\sum_{i=2}^3 t^i & w & -\sum_{i=1}^3 t^i \\ -t^3 & -t^3 & -t^3 & -t^3 & -\sum_{i=2}^3 t^i & -\sum_{i=2}^3 t^i & -\sum_{i=1}^3 t^i & w \end{pmatrix}. \tag{26}$$

Let us start with the eigenvalue $\varphi_0 = (1 - N^{1-2\sigma})/(2^{2\sigma-1} - 1)$ (see Eq. 17): it has algebraic multiplicity $N/2$, so we have to find $N/2$ linear independent eigenvectors $\{\mu_j\}_{j=1}^{\frac{N}{2}}$ of size $N \times 1$, associated to this eigenvalue such that

$$\mathbf{L}\mu_j = \Big(\frac{1 - N^{1-2\sigma}}{2^{2\sigma-1} - 1}\Big)\mu_j, \qquad \forall j = 1, \cdots, \frac{N}{2}. \tag{27}$$

Our ansatz is

$$\mu_j = (0, \cdots, 0, \overbrace{\frac{1}{\sqrt{2}}}^{2j-1}, \overbrace{-\frac{1}{\sqrt{2}}}^{2j}, 0, \cdots, 0), \qquad j = 1, ..., N/2 \tag{28}$$

that is, a vector that has all the entries equal to zero, but those at the position $2j - 1$ an $2j$, that are respectively equal to $+1/\sqrt{2}$ and $-1/\sqrt{2}$, in order to obtain $N/2$ vectors with norm equal to 1. In this case, the left hand side of Eq. 25 becomes

$$(\mathbf{L}\mu_j)_i = \begin{cases} \frac{(-1)^i}{\sqrt{2}}(L_{2j-1,2j-1} - L_{2j-1,2j}), & \text{if } i = 2j-1, 2j, \\ 0, & \text{otherwise .} \end{cases} \tag{29}$$

Expliting the structure of $\mathbf{L}$, for every row $i = 1, ..., N$, we have

$$L_{2j-1,2j-1} - L_{2j-1,2j} \;=\; (-1)^i\Big(w + \sum_{l=1}^{K} 4^{-l\sigma} = \frac{1 - N^{1-2\sigma}}{2^{2\sigma-1} - 1}\Big), \qquad \forall j = 1, ..., N/2.$$

Comparing this expression with (27) we get that our ansatz (28) is correct. In this way we find a set of $N/2$ independent eigenvectors associated to the eigenvalue φ_0.
We are going to proceed analogously for the computation of the eigenvectors related to $\varphi_n = (2^{n(1-2\sigma)} - N^{1-2\sigma})/(2^{2\sigma-1} - 1)$ for $n = 1, ..., K-1$, each with multiplicity $N/2^{n+1}$. This implies that each of them is associated to 2^{K-n-1} linear independent eigenvectors. In particular, we suppose that they have the form

$$\mu_j = (0, \cdots, 0, \overbrace{\frac{1}{\parallel \mathbf{e}_1 \parallel}}^{1+i2^{n+1}}, ..., \overbrace{\frac{1}{\parallel \mathbf{e}_1 \parallel}}^{(i+1)2^{n+1}}, \overbrace{-\frac{1}{\parallel \mathbf{e}_1 \parallel}}^{1+(i+1)2^{n+1}}, ..., \overbrace{-\frac{1}{\parallel \mathbf{e}_1 \parallel}}^{(i+1)2^{n+2}}, 0, \cdots, 0), \qquad i = 0, ..., n-K-1, \qquad j = 1, ..., 2^{K-n-1}, \tag{30}$$

where $\mathbf{e}_1$ is a one vector of size 2^n such that $\parallel \mathbf{e}_1 \parallel = 2^{n/2}$ and its first entries is either at the position $1 + i2^n$, or at the position $1 + (i+1)2^n$ of φ_j with $i = 0, ..., n-K-1$ and $j = 1, ..., 2^{K-n-1}$. Using the same argument discussed above, (25) has the form

$$(\mathbf{L}\mu_j)_i = \begin{cases} \frac{(-1)^i}{2^{\frac{n}{2}}}\Big(\sum_{l=1+i2^n}^{(i+1)2^n} L_{j,l} - \sum_{l=1+2^n(i+1)}^{2^{n+1}(i+1)} L_{j,l}\Big), & \text{if } j = 1 + i2^{n+1}, ..., (i+1)2^{n+2}, \\ 0 & \text{otherwise .} \end{cases} \tag{31}$$

where $n = 1, .., K-1$, and $i = 0, ..., K-n-1$. The previous equation can be further simplified if one recasts the right-hand term of (31) as

$$\begin{aligned} \sum_{l=1+i2^n}^{(i+1)2^n} L_{j,l} - \sum_{l=1+2^n(i+1)}^{2^{n+1}(i+1)} L_{j,l} \;&=\; (-1)^i\Big(w - \sum_{l=1}^{n} 2^{l-1}4^{-l\sigma} + \sum_{l=n+1}^{K} 2^{l-1}4^{-l\sigma}\Big) \\ &=\; (-1)^i\Big(\sum_{l=n+1}^{K} 2^{l(1-2\sigma)}\Big) \\ &=\; (-1)^i\Big(\frac{2^{n(1-2\sigma)} - N^{1-2\sigma}}{2^{2\sigma-1} - 1}\Big). \end{aligned}$$

Also in this case, comparing the obtained result with (30), we get that our ansatz (30) is correct.

Finally, according to the Frobenius-Perron theorem, for the zero eigenvalue with algebraic multiplicity equal to one, the corresponding eigenvector is $\mu_K = \mathbf{e}_1$. In this way we have obtained a complete basis of N linearly independent eigenvectors related to the N eigenvalues, namely they form an orthonormal basis, that is

$$\mu_i\mu_j = \begin{cases} 1, & \text{if } i = j, \\ 0, & \text{if } i \neq j. \end{cases} \qquad \text{and} \;\; \parallel \mu_i \parallel = 1, \qquad \forall i = 1, ..., N. \tag{32}$$

In particular, retaining the simple case $K = 3$, the orthonormal basis of eigenvectors can be written as

$$\mu = \begin{pmatrix} 1/2\sqrt{2} & 1/\sqrt{2} & 1/2 & 0 & 1/\sqrt{2} & 0 & 0 & 0 \\ 1/2\sqrt{2} & 1/\sqrt{2} & 1/2 & 0 & -1/\sqrt{2} & 0 & 0 & 0 \\ 1/2\sqrt{2} & 1/\sqrt{2} & -1/2 & 0 & 0 & 1/\sqrt{2} & 0 & 0 \\ 1/2\sqrt{2} & 1/\sqrt{2} & -1/2 & 0 & 0 & -1/\sqrt{2} & 0 & 0 \\ 1/2\sqrt{2} & -1/\sqrt{2} & 0 & 1/2 & 0 & 0 & 1/\sqrt{2} & 0 \\ 1/2\sqrt{2} & -1/\sqrt{2} & 0 & 1/2 & 0 & 0 & -1/\sqrt{2} & 0 \\ 1/2\sqrt{2} & -1/\sqrt{2} & 0 & -1/2 & 0 & 0 & 0 & 1/\sqrt{2} \\ 1/2\sqrt{2} & -1/\sqrt{2} & 0 & -1/2 & 0 & 0 & 0 & -1/\sqrt{2} \end{pmatrix}. \tag{33}$$

The generalization to larger sizes is straightforward.

We conclude this section observing that

$$\sum_{i=1}^{N} \mu_{ik} = 0, \forall k = 2, ..., N \tag{34}$$

and that

$$\mu_{ik}^2 = \begin{cases} 1/2^{l+1}, & \text{if } i = 2^{l+1}, \text{ with } l = 0, ..., K-1, \\ 0 & \text{if } i \neq 2^{l+1}, \text{ with } l = 0, ..., K-1. \end{cases} \tag{35}$$

VI. EXAMPLES OF APPLICATIONS

In this section we exploit the results found in Secs. IV and V to derive information about several processes which can be defined on the graph $\mathcal{G}$. These are just a few examples for illustrative purposes since, as underlined in Sec. II, the exact knowledge of the whole Laplacian spectrum can be applied in a very wide range of fields and situations.

A. Random Walks

A simple random walk embedded on an arbitrary graph $\mathcal{G}$ is characterized by the transition matrix $\mathbf{P} = \mathbf{W}^{-1}\mathbf{J}$, that is, the probability that, in a given time step, the walker jumps from i to j is $P_{ij} = J_{ij}/w_i$. Now, from the complete knowledge of the Laplacian spectrum one can derive the dynamical properties of the random walker and, in particular, one can calculate the mean time taken by a random walker to *first* reach a given node. This quantity plays a role in real situations such as transport in disordered media, neuron firing, spread of diseases and target search processes (see e.g., [38, 39, 40]). Without loss of generality, we can fix the target site on the node j and focus on the *mean first passage time* (MFPT) from node i to node j, denoted as T_{ij}. According to the definition of MFPT for random walks, we have $T_{jj} = 0$ and, for any $i \neq j$,

$$T_{ij} = \sum_{k=1}^{N-1} P_{ik} T_{kj} + 1 \tag{36}$$

which can be rewritten in matrix form as

$$\bar{\mathbf{T}} = \bar{\mathbf{P}}\bar{\mathbf{T}} + \bar{\mathbf{e}} = \bar{\mathbf{W}}^{-1}\bar{\mathbf{J}}\bar{\mathbf{T}} + \bar{\mathbf{e}}, \tag{37}$$

where $\bar{\mathbf{e}}$ is the $(N-1)$-dimensional unit vector (1, 1, ..., 1); $\bar{\mathbf{T}}$ is the subvector of $\mathbf{T}$ obtained by deleting the j-th entry and whose i-th entry is ${T_{ij}}^2$; $\bar{\mathbf{P}}$, $\bar{\mathbf{W}}$, and $\bar{\mathbf{J}}$ are, respectively, the submatrices of $\mathbf{P}$, $\mathbf{W}$, and $\mathbf{J}$ obtained by deleting the j-th row and j-th column. With some passages it is possible to express T_{ij} in terms of the spectra of $\mathbf{L}$ as (see [26] for a detailed derivation)

$$T_{ij} = \sum_{z=1}^{N} w \sum_{k=2}^{N} \frac{1}{\lambda_k} (\mu_{ik}\mu_{zk} - \mu_{ik}\mu_{jk} - \mu_{jk}\mu_{zk} + \mu_{jk}^2). \tag{38}$$

Next, we can calculate the *average mean time* T_j to first reach the target node j, by averaging T_{ij} over all possible starting sites, namely

$$T_j \equiv \frac{1}{N-1} \sum_{i=1}^{N-1} T_{ij}. \tag{39}$$

---

[2] More precisely, the i-th entry of $\bar{\mathbf{T}}$ is T_{ij} as long as $i < j$, while if $i > j$ the entry corresponding to T_{ij} is the $(i-1)$-th one.

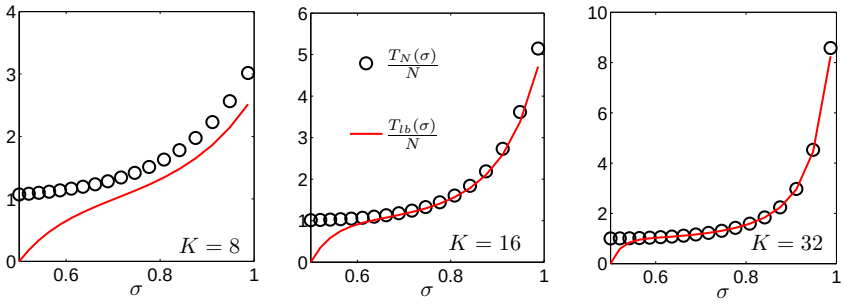

FIG. 4: Trend of T_j/N (circles) and $T_{\rm lb}/N$ (solid line) for $N = 2^K$ with $K = 8, 16, 32$. By plotting the normalized average mean time we get quantities that are roughly comparable as the size is varied. Left panel: for the relatively small size $N = 2^8$ the lower bound $T_{\rm lb}$ does not provide a good estimate for T_j. Central panel: when the size is relatively large as $N = 2^{16}$, the quality of the estimate is far improved. Right panel: when the size is definitely large as $N = 2^{32} \approx 10^9$, $T_j \approx T_{\rm lb}$ almost everywhere.

By exploiting the result of Eq. 38 we can recast the previous expression in terms of the Laplacian eigenvalues and eigenvectors as well, namely (see again [26] for a detailed derivation)

$$\begin{aligned} T_j &= \frac{N}{N-1}\sum_{k=2}^{N}\frac{1}{\varphi_k}\left(s\mu_{jk}^2 - \mu_{jk}\sum_{z=1}^{N} w_z\mu_{zk}\right) \\ &= \frac{N^2}{N-1}w\sum_{k=2}^{N}\frac{1}{\varphi_k}\mu_{jk}^2 \\ &= \frac{N^2}{2(N-1)}w(2^{2\sigma-1}-1)\sum_{l=0}^{K-1}\frac{2^{-l}}{2^{l(1-2\sigma)}-N^{1-2\sigma}} \qquad (40) \\ &= \frac{N^2}{4(N-1)}\frac{2N^{1-2\sigma}(1-2^{2\sigma})+N^{-2\sigma}(2^{2\sigma}-2)+2^{2\sigma}}{2^{2\sigma}-1}\sum_{l=0}^{K-1}\frac{2^{-l}}{2^{l(1-2\sigma)}-N^{1-2\sigma}}, \qquad (41) \end{aligned}$$

where s is the sum of the weighted degrees over all nodes, namely $s = \sum_{i=1}^{N} w_i = \sum_{i=1}^{N}\sum_{j=1}^{N} J_{ij}$. In particular, in this case we have that $s = Nw$, due to the homogeneity among nodes which also implies that T_j is actually independent of j. Moreover, in the second and third lines, we used Eq. 35. The sum appearing in Eq. 41 is not feasible for an explicit, general solution, yet, noticing that

$$\sum_{l=0}^{K-1}\frac{2^{-l}}{2^{l(1-2\sigma)}-N^{1-2\sigma}} \geq \sum_{l=0}^{K-1}2^{l(2\sigma-2)} = \frac{1-N^{2\sigma-2}}{1-2^{2\sigma-2}}, \qquad (42)$$

we can provide T_j with a lower bound, that is,

$$T_j \geq \frac{N^2}{(N-1)}\frac{2N^{1-2\sigma}(1-2^{2\sigma})+N^{-2\sigma}(2^{2\sigma}-2)+2^{2\sigma}}{2^{2\sigma}-1}\frac{1-N^{2\sigma-2}}{4-4^{\sigma}} = T_{\rm lb} \qquad \text{with } \sigma \in \left(\frac{1}{2}, 1\right). \qquad (43)$$

The reliability of this bound is shown in Fig. 4: by varying K and σ we see that the bound is more accurate when the size is large (i.e., $K \gg 1$) and when the pattern of weights is less homogeneous (i.e., σ far from $1/2$). The leading term of $T_{\rm lb}$ scales as

$$T_{\rm lb} \approx \frac{2^{2\sigma}}{(2^{2\sigma}-1)(4-2^{2\sigma})} \times N\left(1-\frac{1}{N^{2\sigma-2}}\right), \qquad (44)$$

which evidences that (at least for large size and for σ far from its boundary values) the MFPT is well approximated by a linear growth with the size N, as corroborated by Fig. 5 (panel a). Moreover, one can show that (see also Fig. 4)

$$T_j \leq T_j(\sigma = 1) \qquad (45)$$

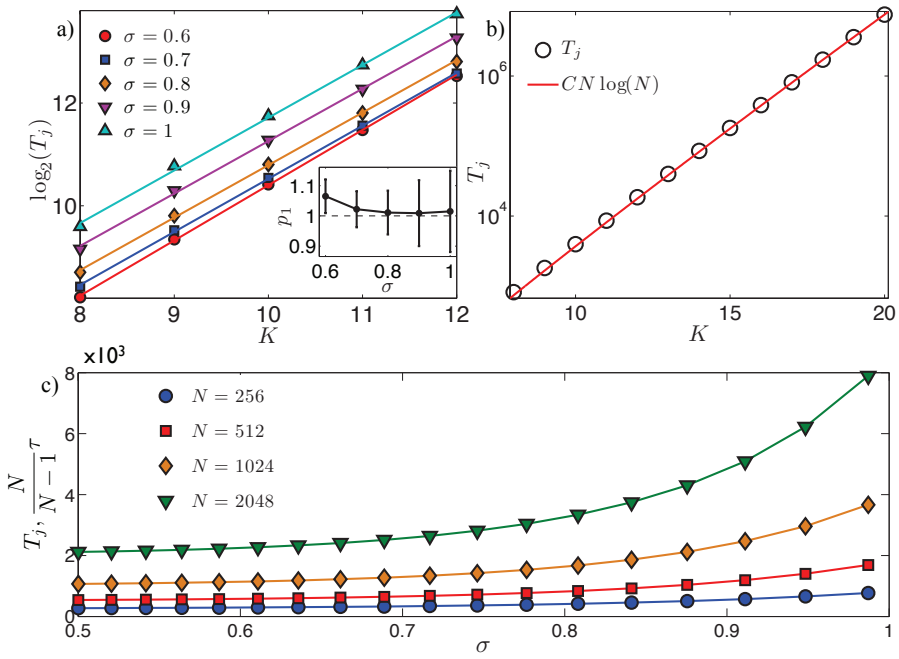

FIG. 5: Panel *a*: Behavior of $\log_2(T_j)$ with respect to $K = \log_2(N)$. Different sets of data, corresponding to different choices of σ, are shown with different symbols, as explained by the legend. Data points are obtained by numerical evaluating Eq. 41, while solid lines represent the best linear fit. In fact, as evidenced in Fig. 4, the lower bound given by $T_{\rm lb}$ in Eq. 43 provides (in the limit of large size and for σ far from its boundary values) a good approximation for T_j and, in turn, in the limit of large size, $T_{\rm lb}$ scales linearly with N as shown in Eq. 44. More precisely, in our fitting function $y = p_1 K + p_2$ we let the fit coefficient free and in the inset we compare the best-fit coefficient p_1 with the unitary value expected from Eq. 44. The comparison is, within the error satisfactory and further highlights that this approximation works better in the central region of the range $\sigma \in (1/2, 1)$. Panel *b*: When $\sigma = 1$ an exact expression for T_j is achievable and here we compare this analytical result, reported in Eq. 47, with the numerical evaluation of T_j from Eq. 41, as the size $N = 2^K$ varies, being $K \in [8, 20]$; notice the semilogarithmic scale plot. The numerical evaluation of T_j (circles) is well approximated by the function $CN\log_2(N)$, where $C \approx 9/25$ (solid line). Panel *c*: Here the MFPT is plotted versus σ and for different choices of the graph size, as indicated by the legend. Data points have been evaluated via the pseudo-inverse Laplacian method [41], while solid lines represent the numerical evaluation of Eq. 41. Notice that, in the limit of large size, T_j corresponds to the global first passage time τ.

and, for $\sigma = 1$, we are able to compute explicitly the sum in Eq. 40. In fact, fixing $\sigma = 1$, it becomes

$$\sum_{l=0}^{K-1} \frac{2^{-l}}{2^{-l} - N^{-1}} = -\frac{1}{2} + \frac{2(3N-1)}{(4N-1)(1-2N)} + K. \tag{46}$$

Plugging this expression in Eq. 41, and posing $\sigma = 1$, we obtain the related exact value of T_j as

$$T_j = \frac{1}{6}\Big(N - \frac{1}{2}\Big)\Big[K + \frac{2(3N-1)}{(4N-1)(1-2N)} - \frac{1}{2}\Big] \approx CN\log_2(N), \qquad \text{as } N \to +\infty, \text{ when } \sigma = 1, \tag{47}$$

where in the last approximation we outlined the leading term being $C \approx 9/25$ (see also Fig. 5, panel *b*).

Therefore, by comparing the approximate results found for $\sigma \in (1/2, 1)$ (see Eq. 44) and the exact results found for $\sigma = 1$ (see Eq. 47), we expect that T_j depends functionally on σ.

In the case the location of the target is unknown, one can still obtain a characteristic time by averaging T_j over all possible target locations, hence getting the so-called *global first passage time*, referred to as τ and defined as

$$\tau \equiv \frac{1}{N(N-1)} \sum_{j=1}^{N} \sum_{\substack{i=1 \\ i \neq j}}^{N} T_{ij} = \frac{1}{N} \sum_{j=1}^{N} T_j. \tag{48}$$

By plugging Eq. 40 into Eq. 48, we get

$$\tau = w \sum_{k=2}^{N} \frac{1}{\varphi_k}, \tag{49}$$

which can be further developed by exploiting the previous results on eigenvalues (see Eq. 17 and 18). However, for the current graph, exploiting the homogeneity among the nodes, one can immediately write

$$\tau = \frac{1}{N}\sum_{j=1}^{N} T_j = \frac{N-1}{N} T_j \approx T_j, \tag{50}$$

where the last passage holds for large N.

To summarize, the MFPT $T_j(\sigma)$ on $\mathcal{G}$ can be bounded as

$$\mathcal{O}(N) \approx T_{\rm lb} \leq T_j(\sigma) \leq T_j(\sigma = 1) \approx \mathcal{O}(N \log N). \tag{51}$$

In general, as expected, $T_j(\sigma)$ grows with σ since when the pattern of weights is more heterogeneous (i.e., σ is large), the graph tends to get disconnected, the mixing time is large and reaching the farthest nodes takes more and more time.

B. Quantum Walks

As stressed above, random walks constitute a basic example of dynamical process affected by the underlying topology. Their quantum-mechanical version, i.e. the quantum walks, constitute an advanced tool for building quantum algorithms and for modeling the coherent transport of mass, charge or energy (see e.g., [42, 43, 44]), and display as well a strong dependence on the topological properties of the embedding structure and, accordingly, much of their properties can be expressed in terms of the Laplacian spectrum. Before deepening this point it is worth reviewing briefly a few definitions (here we just focus on the continuous time version of quantum walks, i.e., continuous-time quantum walks), while we refer to [43] for an extensive treatment.

In such a quantum-mechanical context, the transport has to be formulated in Hilbert space and one assumes that the states $|j\rangle$ representing the nodes span the whole accessible Hilbert space; also, it is assumed that the states are orthonormal and complete, i.e., $\langle i|j\rangle = \delta_{ij}$, and $\sum_i |i\rangle\langle i| = 1$. The dynamics is then governed by a specific Hamiltonian $\mathbf{H}$, such that the Schrödinger equation for the transition amplitude $\alpha_{k,j}(t)$ from state $|j\rangle$ to state $|k\rangle$, reads

$$\frac{d}{dt}\alpha_{k,j}(t) = -i\sum_{l=1}^{N} H_{kl}\alpha_{l,j}(t), \tag{52}$$

where $\hbar$ has been set equal to 1. The squared magnitude of the transition amplitude provides the quantum mechanical transition probability $\pi_{k,j}(t) \equiv |\alpha_{k,j}(t)|^2$. Now, the quantum-mechanical Hamiltonian $\mathbf{H}$ can be identified with the classical transfer matrix, i.e., $\mathbf{H} \equiv \mathbf{L}$ [45].

The performance of the continuous-time quantum walk (CTQW) can be estimated in terms of the return probabilities $\pi_{j,j}(t)$: a quick temporal decay of these probabilities implies a fast transport through the network. In order to make a global statement on the performance, one considers the average return probability $\bar{\pi}$ given by [43]

$$\bar{\pi}(t) = \frac{1}{N}\sum_{j} \pi_{j,j}(t) \geq \left| \frac{1}{N}\sum_{n=1}^{N} e^{-i\lambda_n t} \right|^2, \tag{53}$$

where in the last passage we exploited the Cauchy-Schwarz inequality to get a lower bound for $\bar{\pi}(t)$ which does not depend on the eigenvectors.

For classical diffusion, the long-time limit of the transition probabilities reaches the equipartition value $1/N$. In contrast, due to the unitary time evolution, for CTQW neither $\pi_{i,j}(t)$ nor $\bar{\pi}(t)$ decay to a given value at long times, but rather oscillate around the corresponding long-time average $\bar{\chi}$ which, for $\bar{\pi}(t)$, is given by [43]

$$\bar{\chi} \equiv \lim_{T\to\infty} \frac{1}{T}\int_0^T \bar{\pi}(t)dt = \frac{1}{N}\sum_{n,m} \delta_{\lambda_n,\lambda_m} |\langle j|\mu_n\rangle|^2 |\langle j|\mu_m\rangle|^2. \tag{54}$$

Remarkably, one can obtain a lower bound which does not depend on the eigenvectors and reads as [43]

$$\bar{\chi} \geq \frac{1}{N^2}\sum_{n,m} \delta_{\lambda_n,\lambda_m} \equiv \bar{\chi}_{\rm lb}. \tag{55}$$

Therefore, the full knowledge of the Laplacian spectrum allows estimating (at least via bounds) whether the quantum transport on a given structure propagates relatively fast. Notice that, actually, $\bar{\chi}_{\rm lb}$ just depends on the multiplicities of the distinct eigenvalues.

Indeed, for quantum transport processes the degeneracy of the eigenvalues plays an important role, as the differences between eigenvalues determine the temporal behaviour, while for classical transport the long time behaviour is dominated by the smallest eigenvalue. Situations in which only a few, highly-degenerate eigenvalues are present are related to slow CTQW dynamics, while when all eigenvalues are non-degenerate the transport turns out to be efficient (i.e., it spreads out fast) [43].

In general, an excitation does not stay forever in the system in which it was created; the excitation either decays (radiatively or by exciton recombination) or, e.g., in the case of biological light-harvesting systems, it gets absorbed at the reaction center, where it is transformed into chemical energy. In such cases, the total probability to find the excitation within the network is not conserved. Such loss processes can be modeled phenomenologically by modifying the Hamiltonian $\mathbf{H}$ appearing in Eq. 52. To fix the ideas, we consider networks where the excitation can only vanish at certain nodes, making up a set $\mathcal{M}$ with cardinality $|\mathcal{M}| = M$. These nodes will be called trap-nodes or traps. The new Hamiltonian reads as $\mathbf{H}' = \mathbf{H} + \mathbf{\Gamma}$, where $\mathbf{\Gamma}$ can be written as a diagonal matrix with elements $\Gamma_{ii} = \Gamma$ as long as $i \in \mathcal{M}$ and zero otherwise; Γ represents the (tunable) absorbing rate.

As long as the absorbing rate Γ is small, i.e., $\Gamma \ll 1$, this problem can be treated perturbatively getting that the mean survival probability $\Pi_M(t)$ can be approximated by a sum of exponentially decaying terms:

$$\Pi_M(t) \approx \frac{1}{N-M} \sum_{l=1}^{N} e^{-2\gamma_l t}, \tag{56}$$

where M is the number of traps and γ_l is the imaginary part of the eigenvalue φ'_l of the perturbed Hamiltonian $\mathbf{H}'$ (with approximation at first order), namely $\gamma_l = \Gamma \sum_{m\in\mathcal{M}} |\langle m|\mu_l\rangle|^2$ [43, 46].

Let us now resume the hierarchical graph $\mathcal{G}_K$ and exploit the results obtained in Secs. IV and V to derive an estimate for $\bar{\chi}$ and for $\Pi_M(t)$.

Let us start with $\bar{\chi}$ and notice that the estimate in Eq. 55 only accounts for the degeneracy of the eigenvalues which, as can be seen in Eqs. 17-18, is not affected by σ, but only depends on the system size. As a result, $\chi_{\rm lb}$ does not depend on σ. Moreover, exploiting the expression for φ_k obtained in Eqs. 17-18, as well as the block structure of the graph, we can get that $\chi_{\rm lb}$ for a generic network of size $N = 2^K$ can be obtained from $\chi_{\rm lb}$ referred to the network of size 2^{K-1} with the following recursive equation

$$\chi_{\rm lb}^{(K)} = \frac{1}{N^2}\Big(\chi_{\rm lb}^{(K-1)} + \frac{N^2}{4}\Big), \qquad \text{with } \chi_{\rm lb}^{(1)} = 2. \tag{57}$$

whose solution reads as

$$\chi_{\rm lb}^{(K)} = \frac{N^2+2}{3N^2} \xrightarrow[K\to\infty]{} \frac{1}{3}. \tag{58}$$

We can therefore derive that, no matter the system size and the value of σ, the long time average $\bar{\chi}$ is always finite and larger than 1/3. This means that the coherent transport on $\mathcal{G}_K$ tends to get stuck nearby the starting node. Of course, this stems from the fact that couplings decay fast with the distance among nodes. Actually, localization phenomena also occurs for the classical diffusion, where, as the size N gets larger and larger the mixing time grows exponentially (see [14, 36, 37]) and ergodicity breaks down in the limit $N \to \infty$. However, at finite size, for classical propagation the equipartition is eventually reached, while for the coherent propagation the localization effect is significant already at small size.

Let us now move to $\Pi_M(t)$; according to Eq. 56 it is possible to get a long time estimate in terms of the imaginary part γ_l of the eigenvalues of the perturbed Hamiltonian $\mathbf{H}'$. This can be calculated as follows:

$$\gamma_l = \langle\psi^{(l)}|\mathbf{\Gamma}|\psi^{(l)}\rangle = \Gamma \sum_{i\in\mathcal{M}} [\psi_i^{(l)}]^2 = \Gamma \frac{2^{g_l}}{N} \sum_{i\in\mathcal{M}} (1 - \delta_{\psi_i^{(l)},0}) \tag{59}$$

where in the second passage we exploited the diagonal form of the matrix $\mathbf{\Gamma}$ and in the third passage we exploited the results found in Sec. V. More precisely, $\mathbf{g}$ is a vector, whose entry g_l corresponds to the number of null entries in the eigenvector $\psi^{(l)}$, namely $\mathbf{g} = (0, 0, 1, 1, 2, 2, 2, 2, 3, ..., N-2)$, and $\delta_{x,y}$ is the Kronecker delta in such a way that the summation just returns the number of non-null entries in the eigenvector $\psi^{(l)}$ that match a trap position. For

instance, when $M = 1$, one finds

$$\begin{aligned}
\gamma_1 &= 1/N, \\
\gamma_2 &= 1/N, \\
\gamma_3 &= 2/N,\ \gamma_4 = 0, \\
\gamma_5 &= 4/N,\ \gamma_6 = \gamma_7 = \gamma_8 = 0, \\
\gamma_9 &= 8/N,\ \ldots, \\
&\vdots
\end{aligned}$$

or any other outcome obtained under the permutation of the elements pertaining to the same line (e.g., $\gamma_6 = 4/N, \gamma_5 = \gamma_7 = \gamma_8 = 0$). In general, in the presence of an arbitrary number M ($M \leq N$) of traps, we have $\gamma_1 = \gamma = 2 = M/N$, while for $l > 2$ the value of γ_l depends on the trap arrangement. Moreover, the smallest eigenvalue is null and the second smallest eigenvalue is M/N, whose multiplicity grows with M. Each null eigenvalue corresponds to a block of $\mathcal{G}_K$ which is trap free and this yields to a contribute to $\Pi_M(t)$ which survives even at long times. Therefore, the trap arrangement which maximizes the survival probability is the one where traps are set as close as possible each other, while the trap arrangement which minimizes the survival probability is the one where traps are scattered broadly. This is rather intuitive as the quantum walk tends to remain localized around its starting point in such a way that if traps are assembled within a block, the quantum walk can avoid them as there exists eigenstates living on different blocks, while if each block (even the smallest one, i.e. the dimer) is occupied by at least one trap the quantum walk can not avoid them [47].

C. Dynamics of polymer networks under external forces

Another field where the Laplacian spectrum is extensively exploited is polymer physic and, in particular, as for the investigation of the relationship between the topology of a polymer and its dynamics. To this purpose, the so-called generalized Gaussian structures are conveniently exploited. These are basically a generalization of the Rouse model [7, 48], meant for linear polymer chains, to systems with arbitrary topology. The polymer is modeled as a structure consisting of N beads (each bead corresponding to a node) connected by harmonic springs (we refer to [7] for a discussion of the underlying assumptions).
Understanding how the underlying geometries of polymeric materials affect their dynamic behavior is becoming of increased importance as new polymeric materials with more and more complex architectures are synthesized [7].

Let us consider a set of N beads, all subject to the same friction constant ζ with respect to the sorrounding viscous medium, and connected pairwise by harmonic strings with string constant depending on the "distance" between the nodes connected: for the couple (i, j) it reads CL_{ij}, where C is a suitable constant. The equation describing this phenomenon is the following Langevin equation for to the m-th bead

$$\zeta \frac{d\mathbf{R}_m(t)}{dt} + C \sum_{i=1}^{N} L_{mi} \mathbf{R}_i(t) = \mathbf{f}_m(t) + \mathbf{F}_m(t), \tag{60}$$

where $\mathbf{R}_m(t) = (X_m(t), Y_m(t), Z_m(t))$ represents the position in the space of the m-th bead at time t, $\mathbf{L}$ is the Laplacian matrix associated to the structure of the polymer, $\mathbf{f}_m(t)$ is the thermal Gaussian noise[3], and $\mathbf{F}_m(t)$ is the sum of all external forces acting on the m-th bead.
Now, one can show that, acting (from time $t = 0$ onwards) with a constant external force $F_k(t) = F\delta_{mk}$ on a single bead m of the polymer in the y direction, the mean displacement of a bead turns out to be [7]

$$\langle Y(t) \rangle = \frac{Ft}{N\zeta} + \frac{F}{\rho N \zeta} \sum_{i=2}^{N} \frac{1 - e^{-\rho \varphi_i t}}{\varphi_i} \tag{61}$$

$$= \frac{Ft}{N\zeta} + \frac{F}{2\rho\zeta} \sum_{n=0}^{K-1} \frac{1 - e^{-\rho \varphi_n t}}{2^n \varphi_n}, \tag{62}$$

[3] More precisely, it is assumed that $\langle f_m(t) \rangle = 0$ and $\langle f_{m\alpha}(t) f_{m\beta}(t') \rangle = 2k_B T \delta_{\alpha\beta} \delta_{mn} \delta(t - t')$, where k_B is the Boltzmann constant, T is the temperature, α and β represent the x, y, and z directions.

where $\rho = C/\zeta$ is the bond rate constant, and φ_i is the eigenvalues of matrix $\mathbf{L}$ with φ_K being the unique (for otherwise the polymer would be split in several parts) smallest eigenvalue 0. Also, in Eq. 62 we exploited the results found for the hierarchical graph under study (see Eq. 14).
In the limit of very short time, the terms to be summed up in Eq. 62 can be approximated as $(1 - e^{-\rho\varphi_n t})/(2^n\varphi_n) \approx \rho t 2^{-n}$, hence obtaining the linear scaling

$$\langle Y(t)\rangle \underset{t\to 0}{\approx} \frac{Ft}{\zeta}. \tag{63}$$

Similarly, in the limit of very long times, we can write $(1 - e^{-\rho\varphi_n t})/(2^n\varphi_n) \approx 2^{-n}/\varphi_n$ and, recalling the results in Eq. 50, we get

$$\langle Y(t)\rangle \underset{t\to\infty}{\approx} \frac{Ft}{N\zeta} + \frac{F}{\rho\zeta}\frac{\tau}{w}. \tag{64}$$

Thus, in the limit of short and long times the mean displacement varies linearly with time, with a rate which is independent of σ. Therefore, the most interesting regime is the intermediate one, where the pattern of weights can possibly play a role. In fact, as shown in Fig. 6, this is the case and the resulting displacement is enhanced when the network is more inhomogeneous.

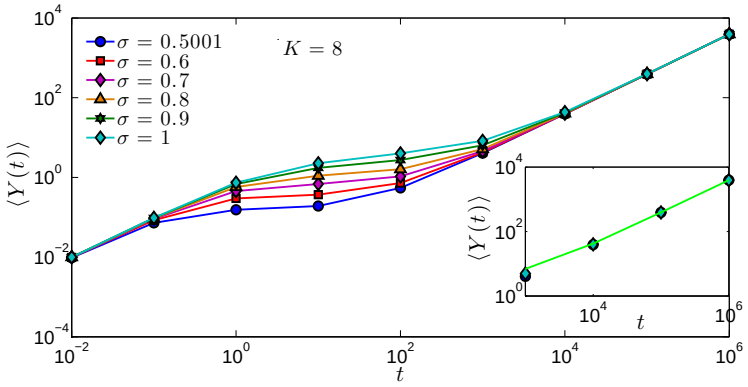

FIG. 6: Trend of $\langle Y(t)\rangle$ as a function of $t \in [10^{-2}, 10^6]$, for $K = 8$ and for different values of $\sigma \in (1/2, 1]$, as shown by the legend. As highlighted analytically (see Eqs. 63 and 64), for short and long times the mean displacement grows linearly with a rate independent of σ. On the other hand, in the intermediate time interval, the rate of growth is sub-linear and slower when the pattern of couplings is more homogeneous. The data points shown here are obtained by numerically evaluating Eq. 62, where we set F/ζ and $F/(2\zeta\varrho) = 1$, lines are guide to eye. The inset shows a zoom on the long-time region where the two extremal cases $\sigma = 0.5001$ and $\sigma = 1$ are compared with the linear law $y = t/N + \tau/w$ (see Eqs. 64, solid line).

When the applied force is harmonic, namely $F_k(t) = Fe^{i\omega t}Y_k(t)$, say along the x direction, the related response function is the so-called complex dynamic (shear) modulus $G^*(\omega)$, whose real, i.e. $G'(\omega)$, and imaginary, i.e., $G''(\omega)$, components are also referred to as the storage and the loss moduli, respectively [7]. In the generalized Gaussian structure model these are given by

$$G'(\omega) = \nu k_B T \frac{1}{N}\sum_{i=2}^{N} \frac{\omega^2}{\omega^2 + (2\gamma\varphi_i)^2}, \tag{65}$$

$$G''(\omega) = \nu k_B T \frac{1}{N}\sum_{i=2}^{N} \frac{2\gamma\varphi_i\omega}{\omega^2 + (2\gamma\varphi_i)^2}, \tag{66}$$

where ν represents the beads per unit volume, φ_i are the non zero eigenvalues of the matrix $\mathbf{L}$ and $\gamma = C/\zeta$ is the monomeric relaxation rate.

Let us now resume the hierarchical graph $\mathcal{G}_K$: this was originally introduced to mimic one dimensional structures with long-range interactions decaying with the distance, thus, the polymer network associated to $\mathcal{G}_K$ can be looked at as a one-dimensional backbone where beads at long distance can as well interact, yet with a vanishing coupling.

Exploiting the results of Sec. IV, Eqs. 65 and 66 can be recast as

$$G'(\omega) = \frac{\nu k_B T (2^{2\sigma-1}-1)^2}{2N} \sum_{n=0}^{K-1} \frac{1}{2^n} \frac{\omega^2}{[\omega(2^{2\sigma-1}-1)]^2 + 4\gamma^2 (2^{n(1-2\sigma)} - N^{1-2\sigma})^2}, \tag{67}$$

$$G''(\omega) = \frac{\nu k_B T (2^{2\sigma-1}-1)}{N} \sum_{n=0}^{K-1} \frac{2^{-n}(2^{n(1-2\sigma)} - N^{1-2\sigma})\omega}{(2^{2\sigma-1}-1)^2\omega^2 + 4(2^{n(1-2\sigma)} - N^{1-2\sigma})^2}. \tag{68}$$

For an arbitrary value of $\sigma \in (1/2, 1]$, the behavior of G' and of G'' has been evaluated numerically and results are shown in Fig. 7. As expected, G' behaves as ω^2 at very low frequencies and as ω^0 at very high frequencies. In the intermediate regime the growth of G' is smoothened and the width of such an intermediate scaling increases with σ. A similar behavior was evidenced for other unweighted networks displaying small-world features in [25, 49]. As for G'', it peaks at around $\omega \approx 1$, the exact value depending on the choice of σ. For relatively small frequencies, G'' is larger when the pattern of weights is more inhomogeneous (i.e., σ large), while for relatively large frequencies G'' is larger when the pattern of weights is more homogeneous (i.e., σ small). In any case the expected scaling $G(\omega) \sim \omega$ and $G(\omega) \sim \omega^{-1}$ is recovered. This is again consistent with the results found for small-world structures in [25, 49].

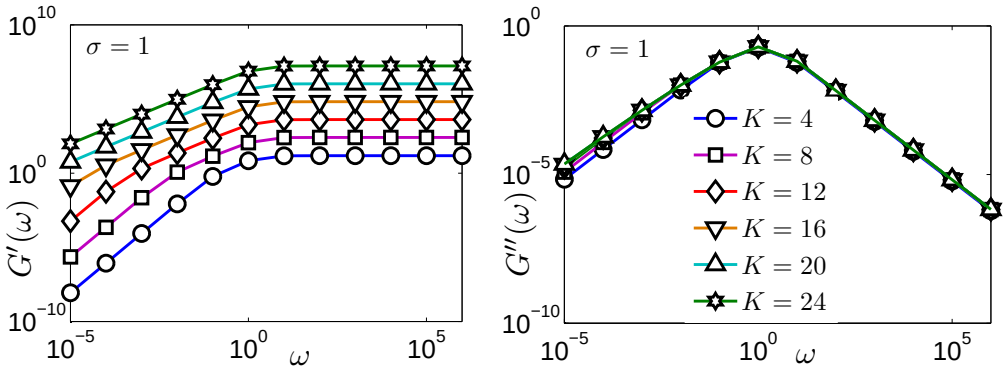

FIG. 7: Gain G' (left panel) and loss G'' (right panel) terms versus $\omega \in [10^{-6}, 10^{6}]$ in a logarithmic scale, for $\sigma = 1$ and for a network of size $N = 2^K$ with $K = 4, 8, 12, 16, 20, 24$, as explained by the common legend. As expected, the gain term G' is monotonically increasing with ω, while the loss term exhibits a peak at intermediate frequencies. Here data are obtained by numerically evaluating Eqs. 67 and 68, where we set $\gamma = 1$ and $\nu k_B T/N = 1$; solid lines are guides to the eye.

For the particular case $\sigma = 1$ we can estimate the asymptotic behaviour of G' by upper-bounding the expression in Eq. 67, that is

$$\begin{aligned} G'(\omega)|_{\sigma=1} &= \frac{\nu k_B T \omega^2}{2} \sum_{n=0}^{K-1} \frac{2^{-n}}{\omega^2 + 4\gamma^2(2^{-n} - 2^{-K})^2} \\ &\leq \frac{N \nu k_B T \omega^2}{8} \sum_{m=0}^{K-1} \frac{2^m}{(2^m-1)^2} \\ &= \frac{N \nu k_B T \omega^2}{8} \left[\log 2 + \frac{2}{\log 2} + \frac{N(6N^2 - 8N + 3)}{2(N^2 - 3N + 1)^2} \right]. \end{aligned} \tag{69}$$

Notice that in the limit of large size the previous passages allow us to derive

$$G'(\omega)|_{\sigma=1} \sim N, \tag{70}$$

as corroborated in Fig. 7.

VII. CONCLUSIONS

In this work we considered the hierarchical graph $\mathcal{G}$ introduced by Dyson and we calculated the exact spectrum of its Laplacian matrix $\mathbf{L}$.

We recall that $\mathcal{G}$ is a weighted fully-connected graph, whose pattern of weights is ruled by the decay rate $\sigma \in (1/2, 1]$. A notion of metric can be defined in such a way that a couple of nodes (i, j) at distance d_{ij} are connected by a link associate to the weight $J_{ij} \sim 4^{-d_{ij}\sigma}$. It turns out that, when $\sigma \to 1/2$ the pattern is more homogeneous, while when $\sigma = 1$ distant nodes are only weakly connected and in the thermodynamic limit they get effectively unconnected.

Here, exploiting the deterministic recursivity through which $\mathcal{G}$ is built, we are able to derive explicitly the whole set of its Laplacian eigenvalues and eigenvectors. In this way, a large class of problems embedded in $\mathcal{G}$ can be addressed analytically. In fact, the Laplacian matrix (also called the admittance matrix or Kirchhoff matrix, see e.g., [15, 16]) is a discrete analog of the Laplacian operator in multivariable calculus and it naturally arises in the analysis of dynamic processes (e.g., random walks) occurring on the graph but also in the investigation of the dynamical properties of connected structures themselves (e.g., vibrational structures and the relaxation modes) [17, 18, 19, 20].

As examples of applications we studied the random walk moving isotropically in $\mathcal{G}$, the continuous-time quantum walk moving in potential given by $\mathcal{G}$, and the relaxation times of a polymer whose structure is described by $\mathcal{G}$.
As for the simple random walk, we found that the average mean time T_j to first reach a given node j depends (super) linearly with the graph size N, the exact dependence being qualitatively affected by σ. In particular, when the pattern of weights is more inhomogeneous T_j grows faster with N, as expected due to the unlikelihood to reach the farthest nodes.
As for the quantum walks, we proved that the long time average, measuring how spread the walker finally gets, is finite and lower bounded by $1/3$ even in the limit of large size. This value has to be compared with the equipartition limit $1/N$ holding for the classical case, suggesting that the coherent transport is not well performing on $\mathcal{G}$. Also, in the presence of absorbing traps, according to their arrangement, surviving stationary states can be established.
Finally, we discusses in the generalized Gaussian framework the dynamics of polymers constituted by beads identified with the nodes of $\mathcal{G}$ and connected by elastic springs whose coupling is identified with the weights encoded by $\mathbf{J}$. Using the Laplacian eigenvalues of $\mathcal{G}$ we estimated the mean displacement, the loss and the storage moduli under the stimulation of an external force. In particular, we found that in the intermediate time (or frequency) domain the response of the polymer is enhanced when the pattern of weights is more inhomogeneous.

The knowledge of the exact spectrum for $\mathcal{G}$ paves the way to further investigations in the phenomenologies related to systems embedded in hierarchical, modular structures. These analysis look particularly interesting given the peculiar behaviours evidenced, e.g., in cognitive and neuroscience [50, 51, 52], and in bioinformatics [53, 54, 55]. For instance, the existence of a wide range of relaxation time scales may shed light on the existence of a number of metastable states for the ferromagnetic Dyson model [14] and on the feasibility of parallel retrieval in Dyson associative networks [56].

Acknowledgements

The authors are grateful to Adriano Barra for enlightening discussions and interactions.
Sapienza Università di Roma and GNFM are acknowledged for financial support.

[1] M. Newman, *Networks: An Introduction* (Oxford University Press, New York, 2012).
[2] L. Gallos, H. Makse, and M. Sigman, Proc. Natl. Acad. Sci. **109**, 2825 (2011).
[3] M. Serrano, M. Boguñá, and A. Vespignani, Proc. Natl. Acad. Sci. **106** (2009).
[4] S. Boccaletti, V. Latora, Y. Moreno, M. Chavez, and D.-U. Hwanga, Physics Reports **424**, 175 (2006).
[5] A. Barrat, M. Barthélemy, R. Pastor-Satorras, and A. Vespignani, Proc. Natl Acad. Sci. **101**, 3747 (2004).
[6] G. Menichetti, D. Remondini, P. Panzarasa, R. Mondragón, and G. Bianconi, PLoS One **9**, e97857 (2014).
[7] A. A. Gurtovenko and A. Blumen, Adv. Polym. Sci. **182**, 171 (2005).
[8] R. Pastor-Satorras and A. Vespignani, Physical Review Letters **86**, 3200 (2001).
[9] E. Agliari, R. Burioni, D. Cassi, and F. Neri, Theor. Chem. Acc. **118**, 855 (2007).
[10] E. Agliari, A. Blumen, and O. Muelken, Physical Review A **82**, 012305 (2010).
[11] A. Barrat, M. Barthélemy, and A. Vespignani, *Dynamical processes on complex networks* (Cambridge University Press, 2008).
[12] E. Agliari and A. Barra, Europhys. Lett. **94**, 10002 (2011).
[13] M. Castellana, A. Decelle, S. Franz, M. Mezard, and G. Parisi, Phys. Rev. Lett. **104**, 127206 (2010).
[14] E. Agliari, A. Barra, A. Galluzzi, F. Guerra, D. Tantari, and F. Tavani, Phys. Rev. Lett. **114**, 028103 (2015).
[15] N. Biggs, *Algebraic Graph Theory* (Cambridge University Press, 1993).
[16] B. Mohar, Discrete Mathematics **109**, 171 (1992).
[17] P. Doyle and L. Snell, *Random Walks and Electric Networks* (Math. Assoc. Amer., Washington, DC, 1984).
[18] Y. Alavi, G. Chartrand, O. R. Oellermann, and A. J. Schwenk, eds., *Graph Theory, Combinatorics, and Applications*, vol. 2 of *Proceedings of the Sixth Quadrennial International Conference on the Theory and Applications of Graphs* (Wiley Press, New York, 1991).
[19] F. R. K. Chung, *Spectral Graph Theory*, 92 (American Mathematical Soc., 1994).
[20] B. Mohar, *Some applications of Laplace eigenvalues of graphs*, vol. Graph Symmetry (Kluwer AC. Press, Dordrecht, 1997).
[21] A. Coolen, The International Meeting on High-Dimensional Data-Driven Science (2016).

[22] K. C. Das, Computers & Mathematics with Applications **48**, 715 (2004).
[23] M. Cosenza and R. Kapral, Phys. Rev. A **46**, 1850 (1992).
[24] C. Jayanthi, S. Wu, and J. Cocks, Phys. Rev. Lett. **69**, 1955 (1992).
[25] H. Liu, M. Dolgushev, Y. Qi, and Z. Zhang, Scientific Reports **5**, 9024 (2015).
[26] Y. Lin and Z. Zhang, Phys. Rev. E **87**, 062140 (2013).
[27] F. J. Dyson, Comm. Math. Phys. **12**, 91 (1969).
[28] M. Girvan and M. Newman, Proceedings of the National Academy of Sciences **99**, 7821 (2002).
[29] L. Donetti and M. Munoz, J. Stat. Mech. p. P10012 (2004).
[30] X. Wang and G. Chen, International Journal of Bifurcation and Chaos **12**, 187 (2002).
[31] L. Lovász, *Combinatorics, Paul Erdös is Eighty*, vol. 2 (Hungary, 1993).
[32] J. M. Harris, J. L. Hirst, and M. J. Mossinghoff, *Combinatorics and Graph Theory*, Undergraduate Texts in Mathematics (Springer, 2008).
[33] X. Chang, H. Xu, and S.-T. Yau, Pacific Journal of Mathematics **273**, 241 (2015).
[34] J. Li, W. C. Schiu, and A. Chang, Applied Mathematics Letters **23**, 286 (2010).
[35] J. Bondy and U. Murty, *Graph Theory with Applications* (MacMillan, New York, 1976).
[36] E. Agliari, A. Barra, A. Galluzzi, F. Guerra, D. Tantari, and F. Tavani, Phys. Rev. E **91** (2015).
[37] F. Tavani and E. Agliari, submitted (2016).
[38] R. Metzler, G. Oshanin, and S. Redner, eds., *First-Passage Phenomena and Their Applications* (World Scientific, 2014).
[39] S. Redner, *A guide to first-passage processes* (Cambridge University Press, 2001).
[40] S. Condamin, O. Bénichou, V. Tejedor, R. Voiturez, and J. Klafter, Nature **450**, 77 (2007).
[41] F. Fouss, A. Pirotte, J.-M. Renders, and M. Saerens, IEEE Transactions on Knowledge and Data Engineering **19** (2007).
[42] J. Kempe, Contemporary Physics **44**, 307 (2003).
[43] O. Muelken and A. Blumen, Physics Reports **502**, 37 (2011).
[44] S. Venegas-Andraca, Quantum Information Processing **11**, 1015 (2012).
[45] E. Farhi and S. Gutmann, Physical Review A **58**, 915 (1998).
[46] E. Agliari, Physica A **390**, 1853 (2011).
[47] E. Agliari, O. Muelken, and A. Blumen, International Journal of Bifurcation and Chaos **20**, 271 (2010).
[48] P. Rouse, J. Chem. Phys. **21**, 1272 (1953).
[49] H. Liu and Z. Zhang, The Journal of Chemical Physics **138**, 114904 (2013).
[50] P. Moretti and M. A. Muñoz, Nature Communications **4**, 2521 (2013).
[51] G. Ódor, R. Dickman, and G. Ódor, Scientific Reports **5**, 14451 (2015).
[52] G. Bardella, A. Bifoni, A. Gabrielli, A. Gozzi, and T. Squartini, arXiv:1601.07574 (2016).
[53] H.-W. Ma, J. Buer, and A.-P. Zeng, BMC Bioinformatics **5**, 199 (2004).
[54] J. Zhao, H. Yu, J.-H. Luo, and Z.-W. Cao, BMC Bioinformatics **7**, 386 (2006).
[55] E. Ravasz, A. Somera, D. Mongru, Z. Oltvai, and A.-L. Barabási, Science **297**, 1551 (20012).
[56] E. Agliari, A. Barra, A. Galluzzi, F. Guerra, D. Tantari, and F. Tavani, Neur. Net. (2015).